Hybrid RANS/LES simulation of a GOX/GCH4 7-element rocket combustor using a non-adiabatic flamelet method

By M. Hansinger, P. Breda, J. Zips, C. Traxinger AND M. Pfitzner

Institut für Thermodynamik, Universität der Bundeswehr München
Werner-Heisenberg-Weg 39, 85577 Neubiberg

For the second time, the SFB-TR40 summer program organized a rocket combustion modeling workshop, where various research groups were invited to employ their numerical tools to simulate flow and combustion in a subscale methane/oxygen rocket combustion chamber. This paper presents the contribution of the Thermodynamics Institute at the Bundeswehr University München. The test case is simulated using a hybrid RANS/LES approach combined with a novel non-adiabatic tabulated combustion model based on the flamelet concept.

1. Introduction

Cryogenic propellant combinations such as liquid oxygen/liquid hydrogen (LOx/LH_2) or storable propellants like MMH/NTO are used in many of today's high performance liquid propellant rocket engines (LRE). Since storable propellants are highly toxic and carcinogenic, handling and operating cost account for a significant share of the total cost and tend to become intolerable, especially in context with new environment regulations. Although LOx/LH_2 offers high specific impulse, the density of hydrogen is low and thereby causes a disadvantageous thrust-to-weight ratio. Moreover, LH_2 requires larger tanks due to additional effort in terms of insulation, which is further reducing its potential from a financial point of view [1]. Therefore, hydrocarbon fuels attract increasing attention in the development of future launchers as they offer lower cost, simpler handling, less pollution and comparable performance. Especially oxygen/methane (O_2/CH_4) is a promising propellant combination: high specific impulse, favorable cooling properties, high density at common tank pressures, low cost both in production and handling, low pollution and safety for human health are methane's interesting key characteristics for its application as LRE fuel [2] [3]. In contrast to LOx/LH_2 engines, where broad experience has been gathered in Europe, the knowledge about O_2/CH_4 combustion at relevant chamber pressures, heat transfer characteristics and injector design is still limited.

Numerical simulations can improve the understanding of injection, mixing and combustion phenomena within the rocket combustor and support the design process. Especially the accurate prediction of wall-heat loads is a crucial aspect for the system design and therefore critically needs to be addressed in the development of the numerical tools. Large eddy simulation (LES) can provide detailed insight in the unsteady reaction flow field, but scale resolving simulation of wall-bounded flows imposes high computational cost due to the required fine resolution of the near-wall region and the thereby limited time step [4]. Therefore, hybrid RANS/LES approaches are a promising tool as they

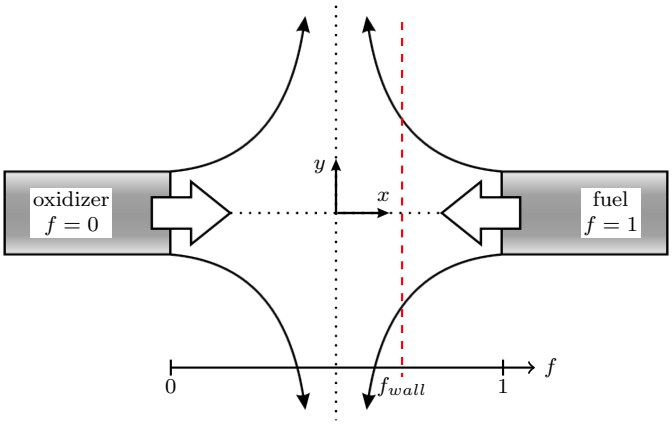

FIGURE 1. Counter-flow diffusion flame configuration with permeable wall.

make use of the advantages of LES in the separated flow region but avoid the restrictions of wall-resolved LES in the near-wall region by employing a RANS model close to walls [5].

The second reason for the high computational effort of the simulation of reacting flows with hydrocarbon fuels is the large number of involved species and reactions. We therefore reduce the computational cost by employing a tabulated combustion model based on the flamelet concept of Peters [6]. The prediction of wall-heat losses requires to incorporate enthalpy losses into the flamelet generation, which is still a field of ongoing research. Here, we transfer a method that has recently been proposed by Ma *et al.* [7] for H_2/O_2 combustion to methane/oxygen combustion. Wall-heat losses are included into the thermo-chemical library, which reflects the effect of reduced enthalpy to the reaction paths and leads to thermal quenching. Special attention is paid to suitable modeling of the transport properties in order to accurately predict the thermal conductivity at wall.

The numerical model consisting of a hybrid RANS/LES approach and a flamelet-based tabulation technique incorporating wall-heat losses is applied to simulate flow and combustion in a sub-scale 7-element rocket combustor operated by Haidn *et al.* [8] at the Institute of Flight Propulsion at TU München. The experiments provide pressure and wall-heat flux measurements which are highly important to evaluate the performance of the numerical tools.

The present study is structured as follows: Tabulated methane/oxygen combustion modeling at elevated pressure incorporating heat-losses is addressed in Sec. 2 and the hybrid RANS/LES method is briefly presented in Sec. 3. Section 5 presents the reference experiment and the numerical setup. Results are shown in Sec. 6 and an outlook on future work is given in Sec. 7.

2. Combustion model

Tabulated combustion models offer the possibility to include detailed reaction mechanisms at reduced computational cost, which is especially promising for hydrocarbon oxidation involving large numbers of species and reactions. Given that chemical time scales are small compared to the turbulent time scales, the structure of a turbulent non-premixed flame can be represented by laminar diffusion flames, henceforth called flamelets. Within the flamelet concept [9], which is valid in the high Damköhler number

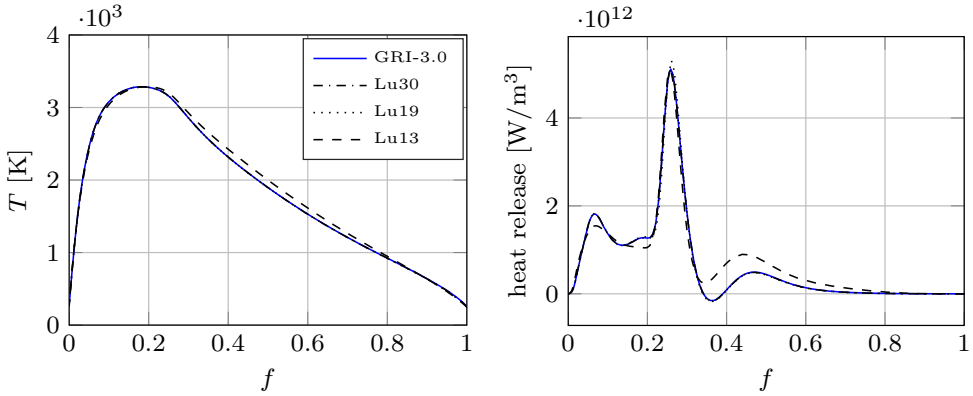

(a) Temperature. (b) Heat release.

FIGURE 2. Performance of the reduced methane mechanisms.

regime, the local flame structure is obtained from one-dimensional counterflow diffusion flame calculations that are stored in a library in a pre-processing step. Within this work, the flamelet model is extended to account for wall-heat loss effects similar to the approach recently employed by Ma *et al.* [7] for H_2/O_2 combustion.

2.1. *Counterflow diffusion flame*

The configuration of a laminar counter-flow diffusion flame as depicted in Fig. 1, can be described as a one-dimensional problem by employing a coordinate transformation to mixture fraction space. Assuming unity Lewis number the steady state governing equations can be written as

$$\frac{\rho\chi}{2}\frac{\partial^2 Y_k}{\partial f^2} = \dot{\omega}_k, \tag{2.1}$$

$$\frac{\rho\chi}{2}\left(\frac{\partial^2 T}{\partial f^2} + \frac{1}{c_p}\frac{\partial c_p}{\partial f}\frac{\partial T}{\partial f}\right) = -\frac{1}{c_p}\sum_{k=1}^{n} h_k\dot{\omega}_k, \tag{2.2}$$

where f is the mixture fraction, ρ the density, T the temperature and c_p the specific heat capacity of the mixture. Denoted by the index k, Y_k, h_k and $\dot{\omega}_k$ are mass fraction, enthalpy and reaction source term of species k. χ_{st} is the scalar dissipation rate at stoichiometry, representing an inverse diffusion time scale. The governing equations are closed using the ideal gas equation of state and the chemical reaction mechanism discussed in Sec. 2.2.

2.2. *Chemical kinetics*

Within the laminar flamelet calculations, an analytically reduced methane mechanism developed by Lu and Law [10] is employed to determine the reaction rates. Despite the tabulated combustion model allows for the use of reaction mechanisms with large number of involved species and reactions, a reduced mechanism with 19 species and 184 reactions is used. This is done to keep the possibility to validate the LES results with a higher fidelity transported PDF method in future work. The mechanism has been derived from the detailed GRI-3.0 [11] using directed relation graph (DRG) [12] and computational singular perturbations (CSP) [13] methods. After a first reduction by DRG, a 30-species mechanism has been obtained. By employing CSP 11 quasi-steady-state

(QSS) species have been identified. The final 19 species (H_2, H, O, O_2, OH, H_2O, HO_2, H_2O_2, CH_3, CH_4, CO, CO_2, CH_2O, CH_3OH, C_2H_2, C_2H_4, C_2H_6, CH_2CO, N_2) are solved via transport equations. The source term calculations involve additional algebraic equations to account for the QSS species, which are solved analytically. Figure 2 demonstrates the performance of the reduced mechanism with respect to the GRI-3.0. The solution of a one-dimensional counterflow diffusion flames at the operating conditions of the BK-S test case shows that both the temperature profile and the heat release agree very well with the detailed mechanism. As a reference, a further reduced 13-species mechanism denoted Lu13 is included in the figure.

2.3. *Transport properties*

Wall-heat flux predictions require a suitable modeling of the thermal conductivity as function of temperature and gas composition. Therefore, the transport properties are implemented according to Kee *et.al* [14]. The single component viscosities μ_k are evaluated from the standard kinetic theory expression including the collision integral and the Lennard-Jones collision diameter. The pure species thermal conductivity is composed of translational, rotational and vibrational contributions. The Wilke semi-empirical formula is used to evaluate the mixture viscosity

$$\mu = \sum_k \frac{\mu_k X_k}{\sum_j \Phi_{k,j} X_j} \tag{2.3}$$

$$\Phi_{k,j} = \frac{\left(1 + \sqrt{\frac{\mu_k}{\mu_j}\sqrt{\frac{M_j}{M_k}}}\right)^2}{\sqrt{8}\sqrt{1 - \frac{M_k}{M_j}}} \tag{2.4}$$

and the mixture thermal conductivity is obtained by

$$\lambda = 0.5\left(\sum_k \lambda_k X_k + \frac{1}{\sum_j \frac{X_k}{\lambda_k}}\right). \tag{2.5}$$

Here, X_k and M_k are the species mole fractions and the molecular weights, respectively. Figure 3 shows the transport properties for a representative flamelet for the four discussed reaction mechanisms. The properties are significantly temperature-dependent and only slight deviations are observed for the 13-species mechanism compared to the reference GRI-3.0.

2.4. *Non-adiabatic flamelet generation*

Wall-heat loss effects are incorporated to the thermo-chemical library by introducing a permeable, isothermal and chemically inert wall at a position f_{wall} in mixture fraction space as schematically shown by the red dashed line in Fig. 1. This corresponds to an additional thermal boundary condition within the domain $T|_{f_{wall}} = T_{wall}$, which is a user defined constant for each specific flamelet. For $f \in (f_{wall}, 1)$ the RHS of Eqs. 2.1 and 2.1 are set to zero. By reducing the wall position f_{wall} starting from the fuel side $f = 1$, the flame is objected to increasing heat loss finally leading to thermal quenching. Figure 4 shows selected profiles for different wall positions as function of mixture fraction. The monotonic decrease in temperature depicted in Fig. 4(a) indicates the wall-heat loss. As long as the wall is sufficiently far away from the flame ($f_{st} = 0.2$), the heat-loss barely affects the maximum flame temperature while imposing a steep temperature gradient

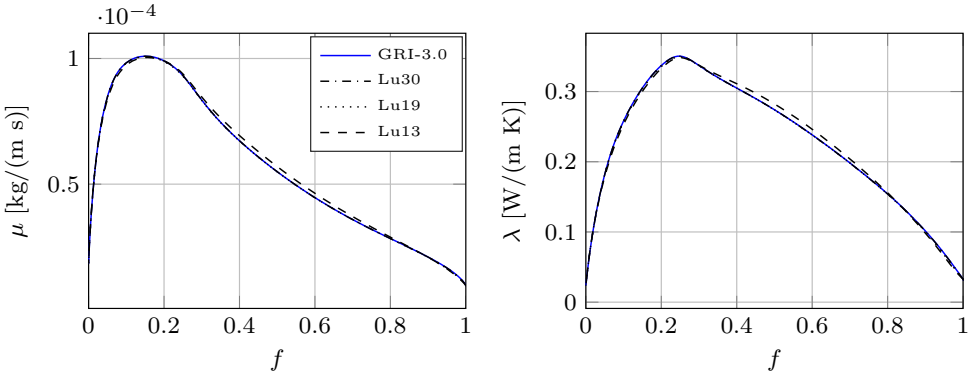

(a) Viscosity. (b) Thermal conductivity.

FIGURE 3. Validation of transport properties.

at the fuel-rich side towards the wall. At approximately $f_{wall} \approx 0.6$, the maximum flame temperature significantly reduces. Concerning the selected species shown in Fig. 4(b), 4(c) and 4(d), one can see that Y_{OH} almost vanishes for wall positions close to the flame. Interestingly, the presence of the wall massively affects the Y_{CO}-Y_{CO2} ratio along the flamelet. With decreasing f_{wall}, the presence of Y_{CO} is strongly reduced while Y_{CO2} becomes the prominent species in the flame.

The range of the tabulated thermo-chemical state is further increased to cover all possible states in the simulation as follows: To prevent situations, where cold pockets of propellants reach a wall with a higher temperature, the mixture composition of the adiabatic flamelet (see Fig. 4, $f_{wall} = 1$) is frozen and the enthalpy is gradually increased. Similarly, the last flamelet before extinction due to wall-heat losses occurs ($f_{wall} = 0.3$) is used to extend the tabulation range towards lower enthalpy values. In a physical sense, this corresponds to a further cooling of the combustion products at frozen composition.

In order to reduce the size of the thermo-chemical library, the database is created using a single value of the scalar dissipation rate. Figure 5 shows that CH_4/O_2 flames at elevated pressure are very robust to strain, as the maximum temperature is fairly constant for a wide range of scalar dissipation rates. Extinction occurs at $\chi_{st} \approx 3 \cdot 10^5$, which is significantly above the values encountered in the present LES study. However, Fig. 5(b) reveals moderate differences in the flame structure also for lower scalar dissipation rates, especially on the fuel-rich side. Hence, the effect of strain is planned to be incorporated into the database for future work although the error is accepted for the present study. Therefore the laminar database is stored as $\Phi = \Phi(f, h)$. Turbulence-chemistry interaction is accounted for by using presumed probability density functions (PDF) and assuming statistical to decompose the joint PDF into a β-PDF and a Dirac function for the enthalpy. Consequently, the final library consists of three dimensions for which transport equations are solved during the LES run.

3. Hybrid RANS/LES model

Accurate prediction of wall-heat fluxes in the LES context implies proper resolution of the boundary layer, which drastically increases the computational effort from $t_{CPU,WF} \approx \sqrt{Re_L}$ for a wall-modeled LES to $t_{CPU,WR} \approx Re_L^{2.7}$ for a wall-resolved LES for a generic boundary layer flow [4]. Considering the high velocities occurring in a typical rocket

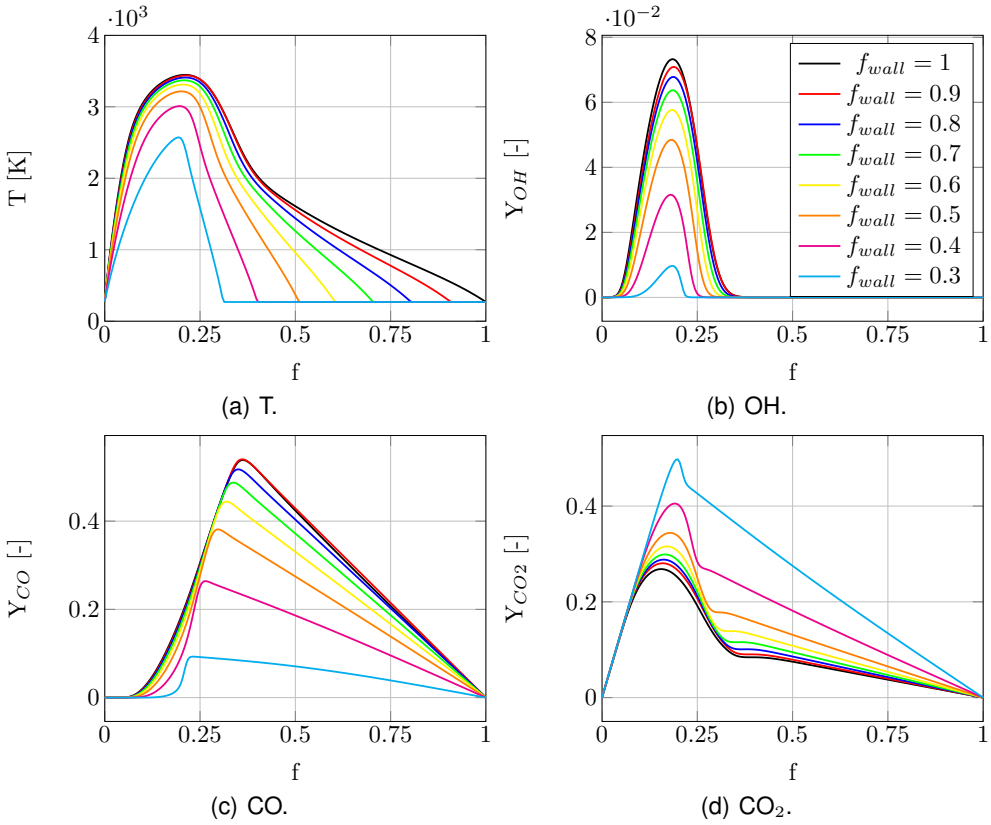

FIGURE 4. Representative flame structure results of one-dimensional flamelet calculations for different wall positions f_{wall} at low scalar dissipation rate $\chi_{st} \approx 1$. The circles in the left figure correspond to the profiles shown in the right one.

combustor and the geometrical size, the computational resources typically do not allow for a sufficiently wall-resolved LES. However, LES is a promising tool to gain further insight in the unsteady mixing and combustion process in the core flow. Hybrid RANS/LES models offer the possibility to employ LES within the free flow, while the near-wall region is covered by a RANS model. Within the present study we use the improved delayed detached-eddy simulation (IDDES) model as proposed by Shur *et al.* [15]. Historically, the method is based on the work of Spalart *et al.* [5], who introduced the concept of detached-eddy simulation (DES). The approach was further refined by Spalart *et al.* [16] to avoid unphysical boundary layer separation that could occur under certain grid-dependent circumstances and was henceforth denoted delayed detached-eddy simulation (DDES). Finally, IDDES combines DDES, where RANS is employed in the whole attached boundary layer with a wall-modeled LES approach, where RANS is only used in a thinner near-wall region. In the hybrid model, the turbulence length-scale is computed by

$$l_{hyb} = \tilde{f}_d\,(1 + f_e)\,l_{RANS} + \left(1 - \tilde{f}_d\right) l_{LES}, \tag{3.1}$$

where l_{RANS} and l_{LES} are the RANS and LES length scales, respectively. The empirical functions $\tilde{f}_d$ and f_e guarantee smooth blending between RANS and LES region and

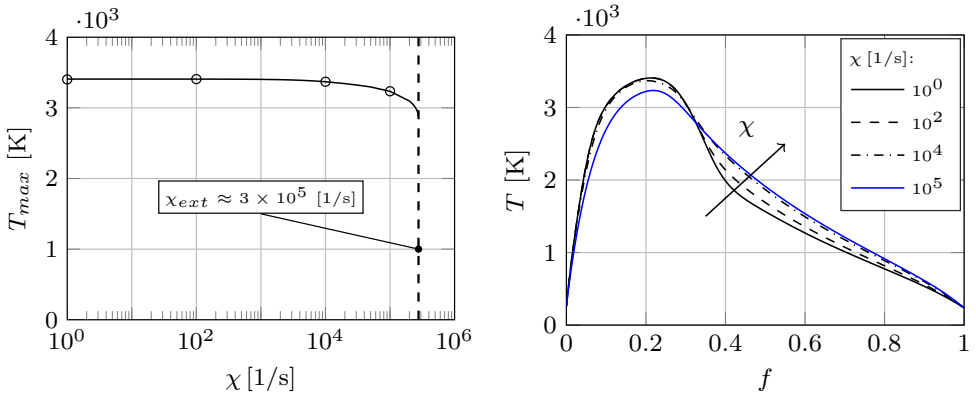

(a) Maximum flame temperature. (b) Temperature profiles.

FIGURE 5. Flamelet structure for varying scalar dissipation rate.

prevent the log-layer mismatch at the interface. Both RANS and LES model can be arbitrary chosen, here we employ the formulation of Shur *et al.* [15] and use a simple Smagorinsky LES model and the one-equation Spalart-Allmaras RANS model [17]. All model constants are set according to Shur *et al.* [15].

4. Governing equations

In Cartesian coordinates x_i and time coordinate t, the filtered conservation equations of mass and momentum read

$$\frac{\partial \bar{\rho}}{\partial t} + \frac{\partial}{\partial x_j}\left(\bar{\rho}\tilde{u}_j\right) = 0, \tag{4.1}$$

$$\frac{\partial}{\partial t}\left(\bar{\rho}\tilde{u}_i\right) + \frac{\partial}{\partial x_j}\left(\bar{\rho}\tilde{u}_i\tilde{u}_j\right) = -\frac{\partial \bar{p}}{\partial x_i} + \frac{\partial}{\partial x_j}\left(2\left(\bar{\mu}+\mu_{sgs}\right)\left(\tilde{S}_{ij} - \frac{1}{3}\tilde{S}_{kk}\delta_{ij}\right)\right). \tag{4.2}$$

The bar $\bar{\star}$ marks the finite-volume filter and a tilde denotes Favre-filtering $\tilde{\star} = \overline{\rho\star}/\bar{\rho}$. ρ, u_i, p, μ and μ_{sgs} are the density, the velocity vector, the pressure, the molecular dynamic viscosity and the SGS viscosity, respectively. δ_{ij} is the Kronecker-Delta and the resolved strain rate tensor reads

$$\tilde{S}_{ij} = \frac{1}{2}\left(\frac{\partial \tilde{u}_i}{\partial x_j} + \frac{\partial \tilde{u}_j}{\partial x_i}\right). \tag{4.3}$$

An additional transport equation is solved for the filtered mixture fraction to retrieve the local mixture composition.

$$\frac{\partial}{\partial t}\left(\bar{\rho}\tilde{f}\right) + \frac{\partial}{\partial x_j}\left(\bar{\rho}\tilde{u}_j\tilde{f}\right) = \frac{\partial}{\partial x_j}\left(\left(\frac{\bar{\mu}}{Sc} + \frac{\mu_{sgs}}{Sc_t}\right)\frac{\partial \tilde{f}}{\partial x_j}\right) \tag{4.4}$$

To model unresolved fluctuations of mixture fraction, a transport equation for its variance is solved according to Kemenov *et al.* [18]:

$$\frac{\partial}{\partial t}\left(\bar{\rho}\widetilde{f''^2}\right) + \frac{\partial}{\partial x_j}\left(\bar{\rho}\tilde{u}_j\widetilde{f''^2}\right) = \frac{\partial}{\partial x_j}\left(\left(\frac{\bar{\mu}}{Sc} + \frac{\mu_{sgs}}{Sc_t}\right)\frac{\partial \widetilde{f''^2}}{\partial x_j}\right) - 2\bar{\rho}\tilde{\chi} + 2\left(\frac{\bar{\mu}}{Sc} + \frac{\mu_{sgs}}{Sc_t}\right)\left(\frac{\partial \tilde{f}}{\partial x_j}\right)^2. \tag{4.5}$$

The scalar dissipation rate χ is decomposed into resolved and SGS contribution [19] as

$$2\bar{\rho}\tilde{\chi} = 2\frac{\tilde{\mu}}{Sc}\left(\frac{\partial \tilde{f}}{\partial x_j}\right)^2 + C_\chi \frac{\mu_{sgs}}{Sc_t}\frac{\widetilde{f''^2}}{\Delta^2}, \tag{4.6}$$

where Δ is the local filter size and the model constant is set to $C_\chi = 2$ [18]. In Eqs. 4.4 and 4.5, the "gradient diffusion" is introduced to describe the turbulent flux. In particular, the molecular (Sc) and turbulent (Sc_t) Schmidt numbers are introduced to connect the diffusion coefficients to the viscosity with the required constants being $Sc = Sc_t = 0.7$ in all simulations.

The Spalart-Allmaras background RANS model requires the solution of a transport equation for a viscosity-like variable $\tilde{\nu}$

$$\begin{aligned}\frac{\partial \tilde{\nu}}{\partial t} + u_j \frac{\partial \tilde{\nu}}{\partial x_j} = C_{b1}\left[1 - f_{t2}\right]\widetilde{S}\tilde{\nu} + \frac{1}{\sigma}\left[\nabla \cdot \left[\left(\nu + \tilde{\nu}\right)\nabla\tilde{\nu}\right] + C_{b2}\left\|\nabla\tilde{\nu}\right\|^2\right] - \\ \left[C_{w1} f_w - \frac{C_{b1}}{\kappa^2} f_{t2}\right]\left(\frac{\tilde{\nu}}{d}\right)^2 + f_{t1}\Delta U^2.\end{aligned} \tag{4.7}$$

From $\tilde{\nu}$ the turbulent viscosity ν_t is computed as $\nu_t = \tilde{\nu} f_{v1}$. The coefficients and empirical functions are implemented in their original form [17].

The simulations are performed with the open-source software package OpenFOAM that has been extended by the required combustion and thermodynamics models. The unstructured finite-volume code employs a PISO algorithm to solve the governing equations. The mass conservation equation is not solved directly but used with the discretized momentum equation to derive a compressible pressure evolution equation guaranteeing mass conservation. This procedure reduces the stiffness of the system in the low Mach number region and allows for larger time steps. Variables are stored in the cell centers and Rhie-Chow interpolation is used to avoid checker-boarding of the pressure. A second-order accurate central differences scheme with the TVD-type van Leer limiter serves for spatial discretization. Temporal integration is performed using a first-order implicit Euler scheme with a maximum global convective Courant number of $Cn = 0.3$.

5. Reference experiment and computational setup

The present numerical approach to simulate methane/oxygen combustion using a hybrid RANS/LES method is employed on a 7-elements subscale rocket combustor, which is experimentally investigated by Haidn *et al.* [8]. The round cross-section chamber, denoted as BKS, has an inner diameter of 30 mm and a total length of 383 mm, including the convergent-divergent nozzle. The cylindric part is 341 mm long. Propellants are injected by seven shear coaxial elements, that are flush-mounted at the faceplate. Oxygen flows through the inner tube with a diameter of 4 mm, methane is provided through the annulus with a channel height of 0.5 mm and the post-tip thickness is 0.5 mm. Figure 6 shows the domain and the injector configuration. The operating point is characterized by a nominal chamber pressure of 18.3 bar and an oxidizer-to-fuel ratio of 2.65. Sonic orifices determine the total mass flow rates of oxygen $\dot{m}_{O2} = 0.211$ kg/m^3 at an injection temperature $T_{O_2} = 259.4$ K and methane $\dot{m}_{CH_4} = 0.08$ kg/m^3 at $T_{CH_4} = 237.6$ K, respectively. The operating conditions are summarized in Tab. 1. BKS is a water-cooled combustion chamber and the thermal loads for each segment are evaluated by a calorimetric method. Pressure and temperature measurements are available at multiple axial

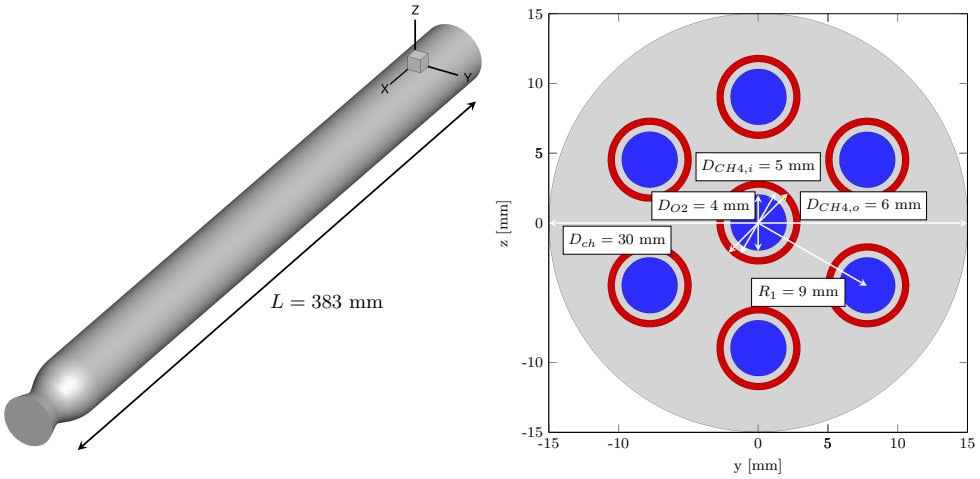

(a) Computational domain. (b) Injection plane.

FIGURE 6. Computational domain and injector configuration.

TABLE 1. Boundary conditions of Haidn *et al.* [8].

O_2			CH_4		
$\dot{m}$ [g/s]	T_{in} [K]	ρ_{in} [kg/m^3]	$\dot{m}$ [g/s]	T_{in} [K]	ρ_{in} [kg/m^3]
211	259.4	27.79	80	237.6	16.03

and radial positions. Since there are no thermocouples at the wall surface, an inverse method is employed to calculate the temperature distribution at the combustor wall from experimental data. This temperature profile is prescribed as thermal boundary condition in the numerical simulations. The faceplate and the injector lips are assumed to be adiabatic no slip walls. At the inlets, constant mass fluxes with a fully-developed velocity profile and the respective temperatures are prescribed for fuel and oxidizer. All values are extrapolated from the domain at the outlet. The computational mesh consists of approximately $64 \cdot 10^6$ cells, the posttip is resolved using 20 cells in radial direction resulting in a minimal grid spacing of 0.025 mm, which is also the minimal axial cell size at the face plate. Further downstream, an axial grading is employed with a maximal axial cell size of 0.75 mm.

6. Results

Figure 7 shows the instantaneous temperature field in a plane perpendicular to the faceplate such that three aligned injection elements are seen. The thin diffusion flames are anchored at the injector lips and show typical Kelvin-Helmholtz instabilities. After approximately 50 mm strong interaction between the flames leads to increased mixing and higher propellant consumption rates. In order to visualize the interaction between the particular flames, Fig. 8 shows instantaneous temperature fields at the axial positions $x = 10$ mm, $x = 50$ mm, $x = 100$ mm and $x = 150$ mm, which are also denoted

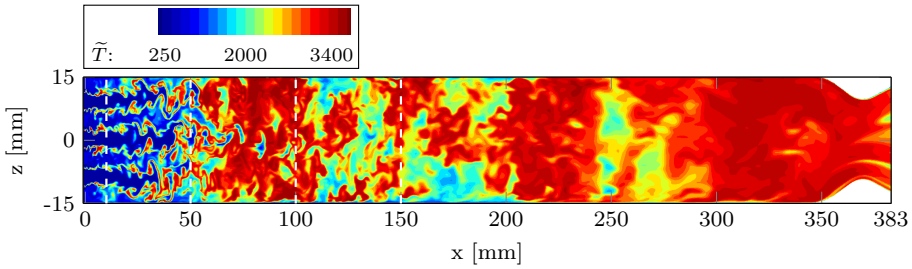

FIGURE 7. Instantaneous temperature field in x-z plane. The view is radially stretched by a factor of 2. The dashed white lines correspond to the axial cuts shown in Fig. 8.

by the white dashed lines in Fig. 7. At $x = 10$ mm, the injector footprint is clearly visible: the flames are relatively thin and slightly wrinkled. However, first interaction with the chamber wall are already visible at this position. The wall-induced shear forces lead to increased mixing at the outer sides of the flames emanating from the outer ring. The high temperature region towards the wall is slightly more diffuse than the inner region. Further downstream, at $x = 50$ mm, the flames are still separated, but the chamber geometry visibly affects the shape of the outer flames. While the central flame still exhibits the round shape induced by the coax-element, the shape of the outer flames adapts to the circular chamber cross section. At the next position, $x = 100$ mm, the flames are no longer separated but the cross section is mostly filled with hot gas and only small colder regions due to incomplete mixing are visible. The thermal boundary layer is very thin, which becomes evident at the next axial position $x = 150$ mm. Here, one can observe the axial growth of the boundary layer as the cold region at the wall is significantly thicker compared to $x = 100$ mm.

The blending function $\tilde{f}_d$ (c.f. Eq. 3.1) is used to visualize the operating mode of the hybrid RANS/LES model. For $\tilde{f}_d = 1$, the model operates in pure LES mode and $\tilde{f}_d = 0$ corresponds to the RANS region. Figure 9 shows $\tilde{f}_d$ in the x-z plane while Fig. 10 provides axial cuts, the first one close to the injector at $x = 5$ mm and the second one further downstream $x = 100$ mm. First, it can be seen that the major part of the domain is covered by LES while only a thin region close to the walls is in RANS mode. Second, the blending between both regions shows a strong gradient and takes place over only a few cells.

7. Conclusion and outlook

During the SFB-TR40 summer program various groups employed their numerical tools to simulate flow and combustion of a 7-element lab-scale GOx/GCH_4 rocket combustion test case. The present contribution applies a relatively novel non-adiabatic flamelet-based tabulated chemistry approach for the efficient simulation of methane/oxygen combustion in rocket combustors. Wall-heat losses are incorporated by an additional thermal boundary condition within the counterflow diffusion configuration. The method is coupled to a hybrid RANS/LES model in order to reduce the vast computational cost of wall-resolved LES. The hybrid approach is the IDDES model of Shur *et al.* [15], where the Smagorinsky model is used within the LES region and the one-equation Spalart-Allmaras model is used in the RANS region. First results indicate that most of the domain is covered by the LES model while only a thin layer at the wall is in RANS mode. This supports the suitability of the model to resolve the large scales of the unsteady injection,

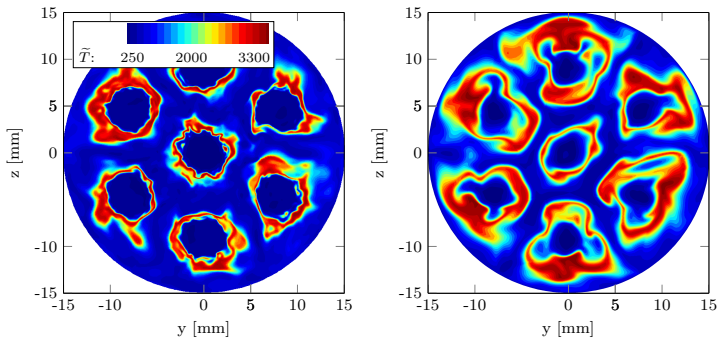

(a) $x = 10$ mm. (b) $x = 50$ mm.

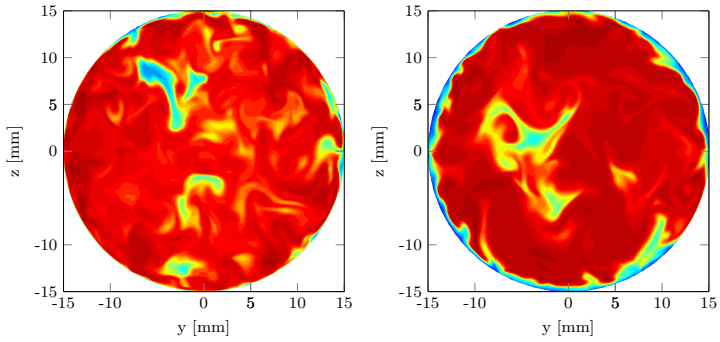

(c) $x = 100$ mm. (d) $x = 150$ mm.

FIGURE 8. Instantaneous temperature field at four axial positions.

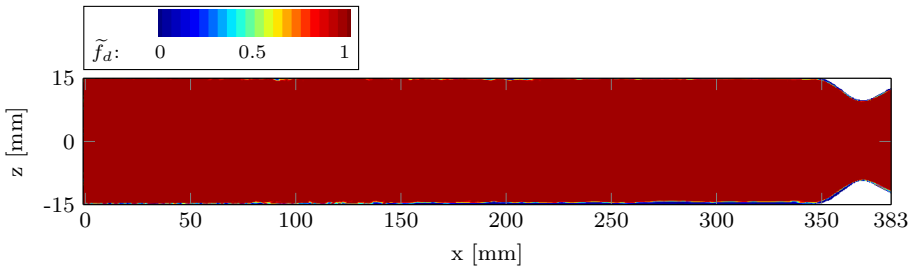

FIGURE 9. Mode of the turbulence model in x-z plane: LES ($\tilde{f}_d = 1$) and RANS ($\tilde{f}_d = 0$) region. The view is radially stretched by a factor of 2.

mixing and combustion processes and avoid the strong grid resolution requirements of wall-resolved LES. Based on these first results, the employed method appears promising and will be further investigated. Additionally, time-averaged results will be analyzed in future work and the performance of the theoretical framework will be evaluated, especially its capability to predict wall-heat fluxes.

Acknowledgments

Financial support has been provided by the German Research Foundation (Deutsche Forschungsgemeinschaft – DFG) in the framework of the Sonderforschungsbereich

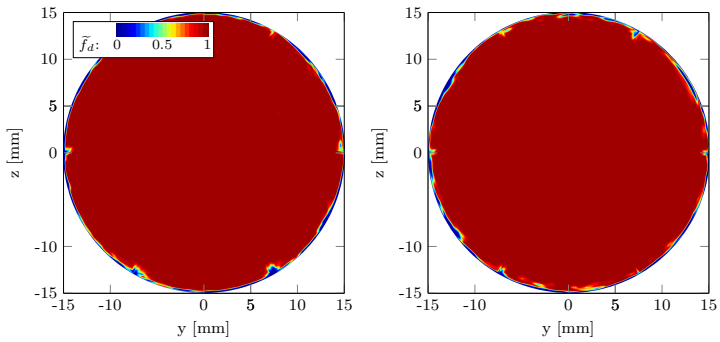

(a) $x = 5$ mm. (b) $x = 100$ mm.

FIGURE 10. Mode of the turbulence model in y-z plane: LES ($\tilde{f}_d = 1$) and RANS ($\tilde{f}_d = 0$) region.

Transregio 40. Computational resources have been provided by the Gauss Centre for Supercomputing e.V. (www.gauss-centre.eu) on the GCS Supercomputer SuperMUC at Leibniz Supercomputing Centre (LRZ, http://www.lrz.de).

References

[1] SUTTON, G. AND BIBLARZ, O. (2001). *Rocket Propulsion Elements*. John Wiley & Sons.

[2] BURKHARDT, H., SIPPEL, M., HERBERTZ, A. AND KLEVANSKI, J. (2008). Kerosene vs Methane: A Propellant Tradeoff for Reusable Liquid Booster Stages. *Journal of Spacecraft and Rockets*, **41**(5), 762–769.

[3] PRECLIK, D., HAGEMANN, G., KNAB, O., MÄDING, C., HAESLER, D., HAIDN, O., WOSCHNAK, A. AND DEROSA, M. (2005). LOX/Hydrocarbon Preparatory Thrust Chamber Technology Activities in Germany. *41st AIAA/ASME/SAE/ASEE Joint Propulsion Conference*.

[4] FRÖHLICH, J. (2006). *Large Eddy Simulation turbulenter Strömungen*. Teubner.

[5] SPALART, P., JOU, W.H., STRELETS, M. AND ALLMARAS, S. (1997). Comments on the feasibility of les for wings, and on a hybrid rans/les approach. In: Liu, C. and Liu, Z. (Eds.), *Advances in DNS/LES*. Greyden Press, First AFOSR International Conference on DNS/LES.

[6] PETERS, N. (1984). Laminar diffusion flamelet models in non-premixed turbulent combustion. *Prog. Energy Combust. Sci.*, **10**, 319–339.

[7] MA, P.C., WU, H., IHME, M. AND HICKEY, J.P. (2017). A Flamelet Model with Heat-Loss Effects for Predicting Wall-Heat Transfer in Rocket Engines. *53rd AIAA/SAE/ASEE Joint Propulsion Conference*, (July), 1–17.

[8] HAIDN, O., CELANO, M.P., SILVESTRI AND ROTH, C. (2015). Transregio SFB-TR40 Test Case BKS-2: 7-Elements Combustion Chamber GCH4/GOX.

[9] PETERS, N. (2004). *Turbulent Combustion*. Cambridge University Press.

[10] LU, T. AND LAW, C.K. (2008). A criterion based on computational singular perturbation for the identification of quasi steady state species: A reduced mechanism for methane oxidation with NO chemistry. *Combustion and Flame*, **154**(4), 761–774.

[11] GRI-MECH 3.0 (2000). *http://www.me.berkeley.edu/gri mech*. University of California at Berkeley.

[12] LU, T. AND LAW, C.K. (2005). A directed relation graph method for mechanism reduction. *Proceedings of the Combustion Institute*, **30**(1), 1333–1341.

[13] LU, T., JU, Y. AND LAW, C.K. (2001). Complex CSP for chemistry reduction and analysis. *Combustion and Flame*, **126**(1-2), 1445–1455.

[14] KEE, R., COLTRIN, M.E. AND GLARBORG, P. (2003). *Chemically Reacting Flow: Theroy & Practice*. Wiley & Sons.

[15] SHUR, M.L., SPALART, P.R., STRELETS, M.K. AND TRAVIN, A.K. (2008). A hybrid RANS-LES approach with delayed-DES and wall-modelled LES capabilities. *International Journal of Heat and Fluid Flow*, **29**(6), 1638–1649.

[16] SPALART, P., DECK, S., SHUR, M., SQUIRES, K., STRELETS, M. AND TRAVIN, A. (2006). A new version of detached-eddy simulation, resistant to ambiguous grid densities. *Theor. Comput. Fluid Dyn.*, **20**(3), 181–195.

[17] SPALART, P. AND ALLMARAS, S. (1994). A one-equation turbulence model for aerodynamic flows. *La Rech. Aerospatiale*, **1**(1), 5–21.

[18] KEMENOV, K., WANG, H. AND POPE, S. (2012). Modelling effects of subgrid-scale mixture fraction variance in les of a piloted diffusion flame. *Combustion Theory and Modelling*, **16**(4), 611–638.

[19] DOMINGO, P., VERVISCH, L. AND VEYNANTE, D. (2008). Large-eddy simulation of a lifted methane jet flame in a vitiated coflow. *Combustion and Flame*, **152**, 415–432.